*Proceedings of the Seventeenth (2007) International Offshore and Polar Engineering Conference*
*Lisbon, Portugal, July 1-6, 2007*

*ISBN 978-1-880653-68-5; ISBN 1-880653-68-0(Set); ISSN 1098-6189 (Set)*

# A Coastline Following Preview Controller for the DELFIMx Vehicle

*Pedro Gomes*[*], *Carlos Silvestre*[*], *Antonio Pascoal*[*], *Rita Cunha*[*]
[*] Institute for Systems and Robotics
Instituto Superior Tecnico
Lisboa, Portugal

## ABSTRACT

This paper describes the development and test in simulation of a coast line following preview controller for the DELFIMx autonomous surface craft (ASC) that takes into account the reference characteristics ahead of the vehicle. The presented solution is based on the definition of an error vector to be driven to zero by the path-following controller. The proposed methodology for controller design adopts a polytopic Linear Parameter Varying (LPV) representation with piecewise affine dependence on the chosen parameters to accurately describe the error dynamics. The controller synthesis problem is formulated as a discrete-time $H_2$ control problem for LPV systems and solved using Linear Matrix Inequalities (LMIs). To increase the path-following performance, a preview controller design technique is used. The resulting nonlinear controller is implemented with the D-Methodology under the scope of gain-scheduling control theory. To build the reference path from laser range finder measurements, an automatic reference path reconstruction technique is presented that employs B-splines computed using least squares coefficient estimation. The final control system is tested in simulation with a full nonlinear model of the DELFIMx catamaran.

KEY WORDS: Path-following, H2 Control, Preview Control, Marine Vehicles, B-splines, Ladar, laser range finder

## INTRODUCTION

Marine biologists and researchers depend on technology to conduct their studies on time and space scales that suit the phenomena under study. Several oceanography missions can be performed automatically by Autonomous Surface Craft (ASC), like bathymetric operations and sea floor characterization. ASC vehicles not only serve research purposes but can also be used for performing automatic inspection of rubblemound breakwaters, as required by the MEDIRES project, (Silvestre *et al.*, 2004). In the scope of this project, the autonomous catamaran DELFIMx, built at IST-ISR, will be used for automatic marine data acquisition. The vessel is a major redesign of the DELFIM Catamaran, developed within the scope of the European MAST-III Asimov project that set forth the goal of achieving coordinated operation of the INFANTE autonomous underwater vehicle and the DELFIM ASC and thereby ensuring fast data communications between the two vehicles.
The DELFIMx craft, depicted in Figure 1, is a small Catamaran 3.5 m long and 2.0 m wide, with a mass of 320 Kg. Propulsion is ensured by two propellers driven by electrical motors. The maximum rated speed of the vehicle with respect to the water is 5 knots. The vehicle is equipped with on-board resident systems for navigation, guidance and control, as well as mission control. Navigation is achieved by integrating motion sensor data obtained from an attitude reference unit and a DGPS (Differential Global Positioning System). Transmissions between the vehicle, its support vessel or the control centre installed on-shore are achieved via a serial radio link. The vehicle has a wing shaped, central structure that is lowered during operations at sea. At the bottom of this structure, a low drag body is installed that can carry acoustic transducers. For bathymetric operations and sea floor characterization, the wing is equipped with a mechanically scanned pencil beam sonar and a sidescan sonar. The paper addresses the design of a laser range finder based coast line following controller to provide DELFIMx with the capability of safely performing automatic inspection of rubblemound breakwaters as is required by the MEDIRES project.

[1]This work was partially supported by Fundação para a Ciência e a Tecnologia (ISR/IST pluriannual funding) through the POS_Conhecimento Program that includes FEDER funds and by project MEDIRES of the AdI.


Fig. 1. The DELFIMx autonomous surface craft

For motion control of autonomous vehicles two strategies arise: trajectory-tracking and path-following. Due to its enhanced performance, which translates into smoother convergence to the path and less demand on the control effort, the path-following approach was chosen. In this paper, the path-following problem is formulated along the lines of the work reported in (Paulino *et al.*, 2006) and (Cunha *et al.*, 2006). The path-following problem can be cast and solved as a regulation problem through the definition of a suitable error vector which depends on both the vehicle variables (velocities, position, and orientation) and the reference (velocities and path). The error vector contains velocity, orientation, and position errors (the position error is defined as the distance between the vehicle's position and its orthogonal projection on the path).

In order to model the error dynamics, a polytopic Linear Parameter Varying (LPV) representation with piecewise affine dependence on the parameters is used. For each region in the vehicle's flight-envelope, a discrete-time $H_2$ controller is synthesized using Linear Matrix Inequalities (LMIs). Since future path references are available, a preview control algorithm is applied. Based on the results presented in (Paulino *et al.*, 2006), a feedforward preview gain matrix is computed. This sort of algorithms are widely used to increase the overall close loop performance, which in this case corresponds to achieving better path-following performance with smoother actuation. Pioneer work on preview control can be found in (Tomizuka, 1976) and references therein. The resulting nonlinear controller is implemented within the framework of gain-scheduling control theory, using the D-Methodology, see (Kaminer *et al.*, 1995). The overall closed-loop system is tested in the MATLAB/SIMULINK simulation environment, using a full nonlinear model of the DELFIMx catamaran with a laser sensor on board.

A fundamental issue underlying the implementation of sensor based coastline following preview controllers is the generation of a smooth reference path from laser measurements. In this paper, the technique adopted exploits the sensor geometry to efficiently build the coast line profile ahead of the vehicle using B-splines. B-spline curves are a good solution since they do not interpolate exactly all the data points but approximate their shape. Details on B-splines can, for example, be found in (Farin, 1997; de Boor, 2001). In addition to being a good representation for the data sets, B-splines have the advantages of being invariant to affine transformation, smoothing noise, and naturally decoupling the x and y coordinates.

The paper is organized as follows. The second section introduces a nonlinear model for the dynamics of the DELFIMx ASC in the horizontal plane. In the third section the problem of coast line following is formulated and a brief introduction of path-dependent error space used to describe the vehicle dynamics is made. The fourth section states the preview control problem. The fifth section describes the methodology adopted for $H_2$ linear controller design where an LMI synthesis technique is applied to affine parameter-dependent systems. The sixth section presents the reconstruction technique used to build the reference path from laser measurements. The seventh section focuses on the implementation of the nonlinear coast line following controller for the DELFIMx ASC. Finally, simulation results obtained with the full nonlinear dynamic model are presented in the last section.

## VEHICLE DYNAMICS

This section briefly presents the model adopted to describe the dynamics of the DELFIMx catamaran in the horizontal plane. The vehicle has two hulls, two propellers driven by electrical motors, and a torpedo-shaped sensor container, attached to the catamaran by a central wing-shaped link. For a comprehensive description of this model, the reader is referred to (Prado, 2002).

Using standard notation in the field, let $\{U\}$ denote the inertial coordinate frame, $\{B\}$ the body fixed coordinate frame attached to the vehicle's center of mass and consider the following vehicle variables:

$^{U}\mathbf{p}_B = [x\ y]^T$ - position of the origin of $\{B\}$ with respect to $\{U\}$;
$\mathbf{v} = [u\ v]^T$ - linear velocity of $\{B\}$ relative to $\{U\}$, expressed in $\{B\}$;
$\psi$ - heading angle that describes the orientation of frame $\{B\}$ with respect to $\{U\}$;
$r$ - angular velocity of $\{B\}$ relative to $\{U\}$, expressed in $\{B\}$.

The vehicle's kinematics can be written as

$$\begin{cases} \dot{\psi} & = & r \\ {}^{U}\dot{\mathbf{p}}_B & = & {}^{U}_{B}R\,\mathbf{v} \end{cases}$$

where ${}^{U}_{B}R$ denotes the rotation matrix from $\{B\}$ to $\{U\}$.
Consider also the generalized variables for the horizontal motion mode given by

$$\boldsymbol{\nu} = \begin{bmatrix} u & v & r \end{bmatrix}^T$$
$$\boldsymbol{\tau} = \begin{bmatrix} X & Y & N \end{bmatrix}^T$$

where $\boldsymbol{\tau}$ denotes the generalized force vector comprising the external forces $[X, Y]$ and moment $N$. Then, the equations of motion for the dynamics can be written in compact form as

$$M\,\dot{\boldsymbol{\nu}} + C\,\boldsymbol{\nu} = \boldsymbol{\tau}, \tag{1}$$

where $M$ is the 2-D rigid body inertia matrix and $C$ the matrix of Coriolis and centripetal terms. The generalized force $\boldsymbol{\tau}$ can be decomposed as

$$\boldsymbol{\tau} = \boldsymbol{\tau}_{add}(\dot{\boldsymbol{\nu}}, \boldsymbol{\nu}) + \boldsymbol{\tau}_{body}(\boldsymbol{\nu}) + \boldsymbol{\tau}_{prop}(\boldsymbol{\nu}, \mathbf{u}), \tag{2}$$

where $\boldsymbol{\tau}_{add}$ denotes added mass terms, $\boldsymbol{\tau}_{body}$ the hydrodynamic forces and moments acting on the body, and $\boldsymbol{\tau}_{prop}$ the forces and moments generated by the propellers as a function of the velocities $\boldsymbol{\nu}$ and of the actuation vector $\mathbf{u} = [n_c\ n_d]^T$. The symbols $n_c$ and $n_d$ stand for the common and differential modes of the propellers' speed of rotation.
The major difficulty faced when modeling a catamaran lies in obtaining an analytical expression for $\boldsymbol{\tau}$. In the current horizontal plane model, the gravitational effect is neglected and the fluid is assumed to be at rest, whereas the dynamic and hydrodynamic effects of the different catamaran components are accounted for in the final expression for $\boldsymbol{\tau}$, see (Prado, 2002) for further details.

## ERROR SPACE

In order to address the path-following problem and convert it into a regulation problem, the vehicle's dynamics are expressed in a conveniently defined error space that naturally describes the dynamic characteristics of the ASC for a suitable flight envelope.

### Tangent and Desired Body Frames

The error space definition requires the introduction of a coordinate frame that relates the vehicle position with the path. This frame, whose $x$ and $y$ axes are constrained to be tangent and normal to the path, respectively, is called the tangent frame $\{T\}$ (see Fig. 3). There is an almost exact correspondence between $\{T\}$ and the well-known Serret-Frenet frame, which, as illustrated in Fig. 2, can only differ on the direction of the normal axis. This is an alternative definition of great practical significance, since it widens the set of paths for which continuity in $\{T\}$ can be guaranteed. In addition to being aligned with

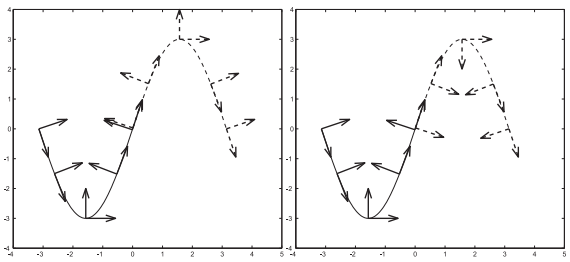

Fig. 2. Tangent and Serret-Frenet frames

the tangent to the path, the frame $\{T\}$ is constrained to move along the path as a function of the vehicle's motion, so that its origin corresponds to the orthogonal projection of the vehicle's position on the path (see Fig. 3).

Given these constraints, it is easy to show that the linear velocity $\mathbf{v}_T = {}^T_U R\, {}^U\dot{\mathbf{p}}_T$ is given by

$$\mathbf{v}_T = V_T \begin{bmatrix} 1 & 0 \end{bmatrix}^T,$$

where $V_T$ is the speed with which $\{T\}$ is moving along the curve, and that the distance $\mathbf{d} = {}^U\mathbf{p}_B - {}^U\mathbf{p}_T$ has no component along the tangent axis, that is,

$${}^T_U R\mathbf{d} = \begin{bmatrix} 0 & d_t \end{bmatrix}^T.$$

As for the angular velocity $r_T$, it is easy to show that it verifies

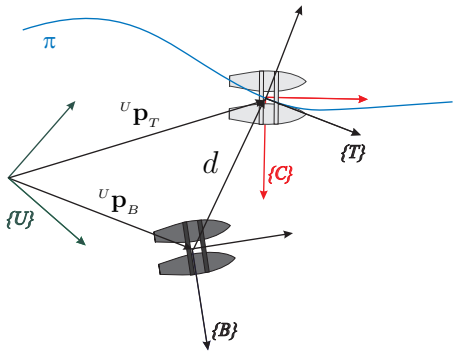


Fig. 3. Coordinate frames and distance to the path

$$r_T = V_T \kappa,$$

where $\kappa$ is the signed curvature, defined for each point on the curve, see (Cunha *et al.*, 2006) for details.

In order to define the error vector, it is necessary to introduce an additional frame: the desired body frame $\{C\}$, which coincides with the tangent frame apart from a $z$-aligned rotation. The angular distance between $\{T\}$ and $\{C\}$ determines the sideslip angle with which the vehicle is supposed to follow a particular curve. Thus, the orientation of frame $\{C\}$ with respect to frame $\{U\}$ can be expressed as

$$\psi_C = \psi_T + \psi_{TC},$$

where $\psi_{TC}$ is the side-slip angle generally defined as $\beta = \arctan(v_C/u_C)$. Notice that $\psi_{TC}$ is highly dependent on the dynamics of the vehicle. However, as will be seen later, the adopted methodology will eliminate the need to explicitly compute the sideslip angle.

## Error Vector Definition and Error Dynamics

Given the foregoing definitions and introducing the reference velocities $\mathbf{v}_R = V_R \begin{bmatrix} 1 & 0 \end{bmatrix}^T$ and $r_R = V_R \kappa$, the following error vector can be considered

$$\mathbf{x}_e = \begin{cases} \mathbf{v}_e = \mathbf{v} - {}^B_T R\, \mathbf{v}_R \\ r_e = r - r_R \\ d_t = \Pi_y\, {}^T_U R\, ({}^U\mathbf{p}_B - {}^U\mathbf{p}_T) \\ \psi_e = \psi - \psi_C \end{cases}, \tag{3}$$

where $\Pi_y = [0\ 1]$. It is straightforward to show that the vehicle follows the path with tangent velocity $\mathbf{v}_r$ and orientation $\psi_C$ if and only if $\mathbf{x}_e = 0$.

Assuming that the references satisfy $\dot{V}_R = 0$ and $\dot{\psi}_{TC} = 0$, the error dynamics can be written as

$$\begin{aligned} \dot{\mathbf{v}}_e &= \begin{bmatrix} \dot{u} + \sin(\psi_e + \psi_{TC})\, \dot{\psi}_e\, V_R \\ \dot{v} + \cos(\psi_e + \psi_{TC})\, \dot{\psi}_e\, V_R \end{bmatrix} \\ \dot{r}_e &= \dot{r} - \dot{r}_R \\ \dot{d}_t &= \sin(\psi_e + \psi_{TC})\, u + \cos(\psi_e + \psi_{TC})\, v \\ \dot{\psi}_e &= r - \kappa \frac{\cos(\psi_e + \psi_{TC})\, u - \sin(\psi_e + \psi_{TC})\, v}{1 - \kappa d_t} \end{aligned} \tag{4}$$

For tracking purposes, the output vector

$$\mathbf{y}_e = \mathbf{v}_e + {}^B_T R \begin{bmatrix} 0 \\ d_t \end{bmatrix}$$

is appended to the system. Note that $\mathbf{y}_e$ results from the combination of velocity and position errors both expressed in body coordinates.

## Error Linearization and Discretization

When the reference path is constrained to verify a trimming condition (which must be feasible for the vehicle in question), the error dynamics becomes an autonomous system with an equilibrium point at $\mathbf{x}_e = 0$ (Cunha *et al.*, 2006). It is well-known that, in 2-D, such a condition is satisfied if the desired path is either a straight line or a circle followed at constant speed ($\dot{V}_R = \dot{r}_R = 0$) and with constant sideslip ($\dot{\psi}_{TC} = 0$). Given that the catamaran is underactuated, it can be shown that the constant parameter vector $\boldsymbol{\xi} = [V_R\ r_R]^T$ completely characterizes a trimming condition and that, imposing this condition on the reference, the error dynamics can be written in compact form as

$$\mathcal{P}(\boldsymbol{\xi}) = \begin{cases} \dot{\mathbf{x}}_e = \mathbf{f}_e(\mathbf{x}_e, \boldsymbol{\xi}, \mathbf{u}) \\ \mathbf{y}_e = \mathbf{g}_e(\mathbf{x}_e, \boldsymbol{\xi}). \end{cases}$$

Defining $\mathbf{u}_C$ as the input vector that satisfies (1) with $\boldsymbol{\nu} = [({}^C_T R \mathbf{v}_R)^T\ r_R]^T$ ($\dot{\boldsymbol{\nu}} = 0$), the linearization of the error dynamics about $(\mathbf{x}_e = 0, \mathbf{u} = \mathbf{u}_C)$ results in the time-invariant system given by

$$\mathcal{P}_l(\boldsymbol{\xi}) = \begin{cases} \delta\dot{\mathbf{x}}_e = A_e(\boldsymbol{\xi})\, \delta\mathbf{x}_e + B_e(\boldsymbol{\xi})\, \delta\mathbf{u} \\ \delta\mathbf{y}_e = C_e(\boldsymbol{\xi})\, \delta\mathbf{x}_e, \end{cases} \tag{5}$$

where $A_e(\boldsymbol{\xi}) = \frac{\partial \mathbf{f}_e}{\partial \mathbf{x}_e}(0, \boldsymbol{\xi}, \mathbf{u}_C)$, $B_e(\boldsymbol{\xi}) = \frac{\partial \mathbf{f}_e}{\partial \mathbf{u}}(0, \boldsymbol{\xi}, \mathbf{u}_C)$, and $C_e(\boldsymbol{\xi}) = \frac{\partial \mathbf{g}_e}{\partial \mathbf{x}_e}(0, \boldsymbol{\xi})$.

For the purposes of control system design, the discrete time equivalent of the linear continuous time model (5) is obtained using a zero-order hold on the inputs. Let $T$ be the sampling time and define, with obvious abuse of notation, the augmented discrete time state $\mathbf{x}_d(k) = [\mathbf{x}_e(k)^T,\ \mathbf{x}_i(k)^T]^T$, where $\mathbf{x}_i(k)$ corresponds to the discrete time integral of $\mathbf{y}_e$. Then, the discrete error dynamics can be written as

$$\mathbf{x}_d(k+1) = A(\boldsymbol{\xi})\mathbf{x}_d(k) + B(\boldsymbol{\xi})\mathbf{u}(k), \tag{6}$$

where $A(\boldsymbol{\xi}) = \begin{bmatrix} e^{A_e(\boldsymbol{\xi})T} & 0 \\ C_e(\boldsymbol{\xi}) & I \end{bmatrix}$ and $B(\boldsymbol{\xi}) = \begin{bmatrix} \int_0^T e^{A_e(\boldsymbol{\xi})\tau} d\tau B_e(\boldsymbol{\xi}) \\ 0 \end{bmatrix}$, for $\boldsymbol{\xi}$ constant.

## PREVIEW PROBLEM FORMULATION

Better path-following performance with limited bandwidth compensators can be achieved by taking into account, in the control law, the characteristics of the reference path ahead of the vehicle. The technique used in this paper to develop a tracking controller amounts to introducing a dynamic feedforward block, which is fed by future path disturbances.

With the objective of including this preview component in the discrete time error space dynamics (6), assume that the catamaran moves with

constant speed along a given reference path that results from the concatenation of straight lines and arcs of circumference. A detailed analysis of the error dynamics (4) suggests the introduction of a perturbation term that results from the discontinuity in the angular velocity $r_R$. Assuming that each path segment concatenation occurs at time $t_i$, the derivative of $r_R$ can be written as

$$\dot{r}_R(t) = \sum_i \delta(t - t_i)(r_R(t_i^+) - r_R(t_i^-)),$$

where $\delta(t)$ is the Dirac delta function. From (5), the resulting linear error dynamics can be written as

$$\delta\dot{\mathbf{x}}_e = A_e(\boldsymbol{\xi})\delta\mathbf{x}_e + B_e(\boldsymbol{\xi})\delta\mathbf{u} + W\delta w, \tag{7}$$

with injection matrix $W = \begin{bmatrix} 0 & 0 & -1 & 0 & 0 \end{bmatrix}^T$. The corresponding discretization is given by

$$\mathbf{x}_d(k+1) = A(\boldsymbol{\xi})\mathbf{x}_d(k) + B(\boldsymbol{\xi})\mathbf{u}(k) + B_1(\boldsymbol{\xi})s(k), \tag{8}$$

where $B_1(\boldsymbol{\xi}) = [(e^{A_e(\boldsymbol{\xi})T}W)^T, 0]^T$ is obtained from the impulse invariant discrete equivalent of the injection matrix $W$. It is assumed that the sampling period is sufficiently small to consider the reference path changes synchronized with the sampling time and therefore the perturbation $s(k)$ can be written as

$$s(k) = r_R(t_k^+) - r_R(t_k^-).$$

Assuming a preview length of $p$ samples, let $\mathbf{x}_s(k) = [s(k), s(k+1), ..., s(k+p)]^T \in \mathbb{R}^{(p+1)\times 1}$ be the vector containing all the preview inputs at instant $k$. Then, the discrete time dynamics of vector $\mathbf{x}_s(k)$ can be modeled as a FIFO queue given by

$$\mathbf{x}_s(k+1) = D\mathbf{x}_s(k) + B_s s(k+p+1), \tag{9}$$

where

$$D = \begin{bmatrix} 0 & 1 & 0 & \cdots & 0 \\ 0 & 0 & 1 & \cdots & 0 \\ \vdots & \vdots & \ddots & \ddots & \vdots \\ 0 & 0 & 0 & \ddots & 1 \\ 0 & 0 & 0 & \cdots & 0 \end{bmatrix}, \quad B_s = \begin{bmatrix} 0 \\ 0 \\ \vdots \\ 0 \\ 1 \end{bmatrix},$$

and the augmented system with state $\mathbf{x}(k) = \begin{bmatrix} \mathbf{x}_d(k)^T & \mathbf{x}_s(k) \end{bmatrix}$ can be written as

$$\mathbf{x}(k+1) = \bar{A}\mathbf{x}(k) + \bar{B}_s s(k) + \bar{B}\mathbf{u}(k), \tag{10}$$

where

$$\bar{A} = \begin{bmatrix} A & H \\ 0 & D \end{bmatrix}, \quad \bar{B}_s = \begin{bmatrix} 0 \\ B_s \end{bmatrix}, \quad \bar{B} = \begin{bmatrix} B \\ 0 \end{bmatrix},$$

and $H = [B_1, 0, 0, \cdots, 0]$ represents the injection matrix of the preview signals into the error dynamics. Notice that the $D$ matrix is stable and therefore the augmented system (10) preserves the stabilizability and detectability properties of the original plant.

## DISCRETE TIME CONTROLLER DESIGN

This section briefly describes the LMI-based methodology that was adopted to solve the problem of discrete time state feedback $H_2$ preview control for polytopic LPV systems (Ghaoui and Niculescu, 1999; Takaba, 2000). In what follows, the standard set-up and nomenclature used in (Zhou *et al.*, 1995) is adopted, leading to the state-space feedback system represented in Fig. 4. Consider the generalized LPV system $\mathbf{G}(\boldsymbol{\xi})$, defined as a function of the slowly varying parameter vector $\boldsymbol{\xi}$. It is assumed that $\boldsymbol{\xi}$ is in a compact set $\Theta \subset \mathbb{R}^q$. Suppose that the parameter set $\Theta$ can be partitioned into a family of regions that are compact closed subsets $\Theta_i$, $i = 1, \ldots, N$ and cover the desired ASC

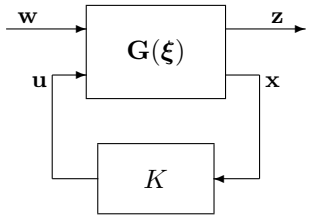


Fig. 4. Feedback interconnection

flight envelope. In the $ith$ parameter region $\Theta_i$, the dynamic behavior of the closed-loop system admits the realization

$$\begin{cases} \mathbf{x}(k+1) = A(\boldsymbol{\xi})\mathbf{x}(k) + B_w(\boldsymbol{\xi})\mathbf{w}(k) + B(\boldsymbol{\xi})\mathbf{u}(k) \\ \mathbf{z}(k) = C_z(\boldsymbol{\xi})\mathbf{x}(k) + E(\boldsymbol{\xi})\mathbf{u}(k), \quad \mathbf{u}(k) = \mathrm{K}\mathbf{x}(k), \end{cases} \tag{11}$$

where $\mathbf{x}(k)$ is the state vector. The symbol $\mathbf{w}(k)$ denotes the input vector of exogenous signals (including commands, disturbances and preview signals), $\mathbf{z}(k)$ is the output vector of errors to be reduced during the controller design process, and $\mathbf{u}(k)$ is the vector of actuation signals. Matrices $A(\boldsymbol{\xi})$, $B_w(\boldsymbol{\xi})$, $B(\boldsymbol{\xi})$, $C_z(\boldsymbol{\xi})$, and $E(\boldsymbol{\xi})$ are affine functions of the parameter vector $\boldsymbol{\xi} = [\xi_1, \ldots, \xi_q]^T \in \Theta_i$, e.g. $A(\boldsymbol{\xi}) = A^{(0)} + \xi_1 A^{(1)} + \ldots + \xi_q A^{(q)}$. The generalized affine parameter-dependent system $\mathbf{G}(\boldsymbol{\xi})$ consists of the plant to be controlled, together with appended weights that shape the exogenous and internal signals and the preview dynamics presented in Section IV.

Given $\mathbf{G}(\boldsymbol{\xi})$, an LMI approach for the synthesis of state feedback $H_2$ controllers for polytopic systems is used to compute $K = [K_d, K_s]$, where $K_d$ and $K_s$ represent the state feedback and feedforward gain matrices respectively, see (Ghaoui and Niculescu, 1999; Paulino *et al.*, 2006) for further details.

For augmented discrete time dynamic systems that include large preview intervals $p > 50$, the controller synthesis technique proposed in (Ghaoui and Niculescu, 1999) leads to LMI optimization problems involving a large number of variables, which cannot easily be solved using the tools available today. To overcome this limitation, an alternative algorithm for the computation of the feedforward gain matrix is adopted that exploits the particular structure of the augmented preview system, see (Paulino *et al.*, 2006).

## REFERENCE PATH GENERATION

To generate the reference path, a laser range finder was attached to the vehicle for coastline data acquisition. This single beam laser range finder, installed in a fixed position on the vehicle, measures the distance between the vehicle and the coastline at a frequency of 100Hz. As the vehicle moves, new coastline points are acquired (see Fig. 5) and stored in a buffer. A coastline profile can then be computed based on the laser data buffer. This curve is dynamic in the sense that it changes as new samples enter the buffer. These new samples can be located after or before the last sample acquired, because the coastline data acquisition process depends on the vehicle's attitude and linear position. For example see Fig. 5, where the vehicle's motion causes a point located at the beginning of a coastline profile to be acquire afterwards.

The dependence of the coastline data acquisition process on the vehicle's motion, makes the coastline following problem harder to solve. Notice that the reference path generation can be simplified by using a ladar, which is able to measure the entire coastline profile several times per second, instead of a laser range finder mounted in a fixed position on the vehicle. Note that in the later case the coastline curve built from sensor measurements can change dramatically with time as new data enters the buffer.

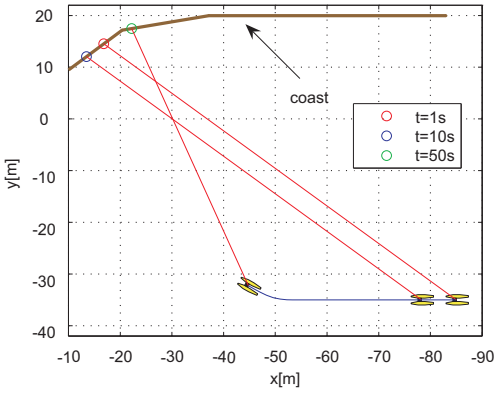


Fig. 5. Coast laser data acquisition

The proposed methodology requires the determination of a reference path parallel to that synthesized from the laser data buffer. Both curves are dynamically updated as new coastline measurements are added to the data buffer, while the vehicle moves along the path.

In order to obtain less demanding engine actuation and still achieve good coastline following performance, the reference path fed into the controller should be smooth and present a shape similar to that of the coastline profile in the presence of noise in the data acquisition process and irregular coastline profiles.

To obtain a coastline profile estimate from laser data sets, B-spline curves are a good solution since they do not interpolate exactly all the data points but approximate their shape. Details on B-splines can, for example, be found in (Farin, 1997). In addition to being a good representation for the data sets, B-splines have the advantages of being invariant to affine transformations, smoothing noise, and naturally decoupling the x and y coordinates. Usually, B-splines of an order of three or four provide a sufficiently accurate approximation. Higher order curves allow higher spatial frequency shapes to be modeled, but also require more computations. In our case order four was found to be a good compromise between the computational requirements and the approximation accuracy of the resulting B-spline.

## Smooth Curves: B-splines

A B-spline curve is a function defined by polynomials obtained from the linear combination of basis functions. Consider the following B-spline definition

$$\begin{aligned} x(l) &= \sum_{k=0}^{N} c_{x,k}\, B_{k,D}(l) \\ y(l) &= \sum_{k=0}^{N} c_{y,k}\, B_{k,D}(l) \end{aligned}$$

where $l$ is the domain parameter, $c_{x,k}$ and $c_{y,k}$ are the $k\,th$ control points (or basis coefficients) for the $x$ and $y$ splines, respectively, $B_{k,D}(l)$ represents the $k\,th$ basis function (or blending function) of order $D$ (and degree $D-1$), and $N+1$ is the number of control points. This curve is built for a given domain partition defined by the knot vector $[l_0, l_1, \ldots, l_N]$ (there is a control point associated to each knot). In the present case we considered non-uniform B-splines, parameterized by the arc length $l$, with basis functions defined by the so-called Carl de Boor formulas (de Boor, 2001)

$$\begin{aligned} B_{k,1}(l) &= \begin{cases} 1 & l_k \le l < l_{k+1} \\ 0 & \text{otherwise} \end{cases} \\ B_{k,d}(l) &= \frac{l - l_k}{l_{k+d-1} - l_k}\, B_{k,d-1}(l) + \\ &\quad + \frac{l_{k+d} - l}{l_{k+d} - l_{k+1}}\, B_{k+1,d-1}(l). \end{aligned}$$

where $d = 2, \ldots, D$. The shape of the curve can be easily adjusted by proper choice of the coefficients and the knots vector. In the following $x'(l)$ denotes $\frac{\partial}{\partial l} x(l)$.

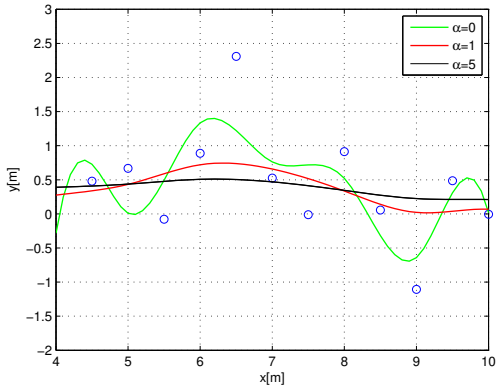


Fig. 6. Impact of $\alpha$ in the curve profile

When adjusting a curve to noisy or high irregular data sets, one must prevent overfitting which can cause near interpolation of the data leading to high spatial frequency references. Methods for obtaining a smooth spline estimate can be found in the literature, (Flickner *et al.*, 1994). In the following we propose a technique to determine the curve coefficients through minimization of a simple least squares cost functional. Let $(\tilde{x}_j, \tilde{y}_j)$ denote the $jth$ sample point and $l_j$ the respective arc length parameterization. Then, the cost functional for $x$ coordinate can be written as

$$J = \frac{1}{2} \sum_j \left[ (x(l_j) - \tilde{x}_j)^2 + \alpha\, x'(l_j)^2 \right].$$

A similar procedure is applied to the $y$ coordinate. The proposed technique introduces in the cost functional an extra smoothing parameter $\alpha$, that weights the derivative of the curve with respect to the parameter $l$. The impact of $\alpha$ on the shape of resulting curve is illustrated in Fig. 6. The spline coefficients $\mathbf{c}_x = [c_{x,0} \ldots c_{x,N}]^T$ are then obtained from the least squares solution

$$\mathbf{c}_x = R^{-1}\, \mathbf{r} \tag{12}$$

where the matrix $R$ and vector $\mathbf{r}$ are given by

$$R = \sum_j \begin{bmatrix} B_0(l_j)^2 + \alpha B_0'(l_j)^2 & \ldots & B_0(l_j) B_N(l_j) + \alpha B_0'(l_j) B_N'(l_j) \\ \vdots & & \vdots \\ B_N(l_j) B_0(l_j) + \alpha B_N'(l_j) B_0'(l_j) & \ldots & B_N(l_j)^2 + \alpha B_N'(l_j)^2 \end{bmatrix}$$

$$\mathbf{r} = \sum_j \begin{bmatrix} B_0(l_j)\tilde{x}_j & B_1(l_j)\tilde{x}_j & \ldots & B_N(l_j)\,\tilde{x}_j \end{bmatrix}^T$$

and the index $D$ in $B_{k,D}$ was omitted for the sake of simplicity.

## Path Generation Methodology

The first step for the reference path generation, consists of computing the coastline profile. Assuming that the laser data samples $(\tilde{x}_j, \tilde{y}_j)$ are sorted in the buffer according to a proximity criterion, the B-spline for the coastline profile can be computed using (12). The second step is to compute the so called offset curve from the coastline profile. This curve, that corresponds to the reference path that the vehicle should follow, is displaced from the coastline profile by a constant offset, the safety distance $s_D$, in the direction of the curve's normal. Different techniques to compute the offset curve can be found in the literature, see (Lee *et al.*, 1996) for an in depth survey of the area. In the following, we present a simple technique to approximate the offset curve that solves the problem at hand.

The main idea consists of using a simple B-spline interpolation method to approximate the offset curve. A finite set of sample points are generated on the exact offset curve and then interpolated resorting to a fourth order B-spline to generate the reference path.

Given the coastline profile $C(l) = (x(l), y(l))$, its exact offset curve $C_\Gamma(l) = (x_\Gamma(l), y_\Gamma(l))$ can be written as

$$C_\Gamma(l) = C(l) + s_D \mathbf{n}(l), \quad \mathbf{n}(l) = \frac{1}{\sqrt{x'(l)^2 + y'(l)^2}} \left[x'(l),\ -y'(l)\right]^T \tag{13}$$

where $\mathbf{n}(l)$ represents the unit vector normal to $C(l)$. For B-splines, the curve derivatives $x'(l)$ and $y'(l)$ are analytical expressions of the basis functions derivatives and curve coefficients.

For convex sections of the coastline profile, within which the local radius of curvature is no greater than the safety distance, the sample offset points lead to an undesired shape generated by offset vectors $\mathbf{o}(l_i) = s_D \mathbf{n}(l_i)$ that intersect each other. The simplest solution to overcome this problem consists of ignoring those vectors in the generation of the reference path. Fig. 7 shows a typical case of a

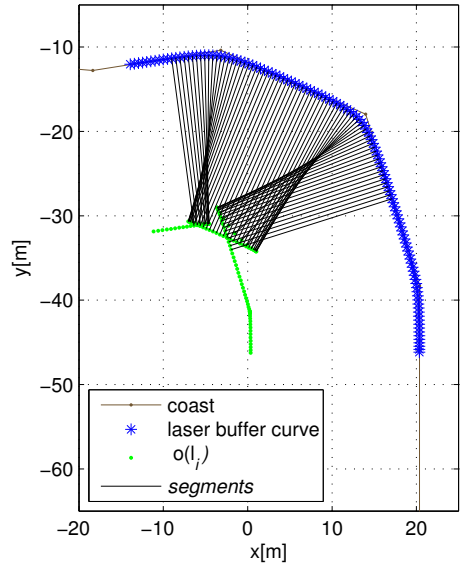


Fig. 7. Coastline convex section

coastline convex section where the local radius of curvature is less than the safety distance. In the figure, the curve identified by the green marks contains an undesired section that results from the intersection of the offset vectors.

The algorithm developed to build the reference path from laser data can be summarized as follows:

- Store each new laser data sample in the buffer and sort it according to a proximity criterion.
- Compute the coastline profile from laser data and append a straight line segment at the end of the curve. This line segment, that is connected to the coastline profile, is aligned with the last 15 control points of the latter.
- Sample the coastline profile and the appended line segment uniformly in $l$ and compute the corresponding offset vectors $\mathbf{o}(l_i)$.
- Remove the offset vectors that intersect each other.
- Compute the B-spline reference path using the control points defined by the remaining offset vectors.

Fig. 8 displays two different phases of the reference path building procedure. The figure on the left contains the results of a first stage of the algorithm where few data points are available. In the figure the appended straight line segment can be easily identified. The righthand side figure shows a posterior phase of the process and attests the quality of the proposed algorithm. Notice also how the proposed technique is able to handle laser occlusions.

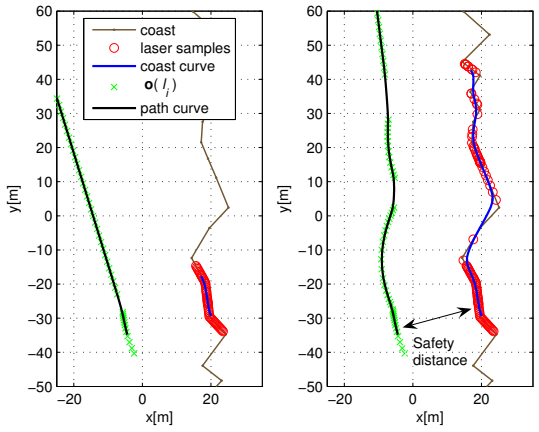


Fig. 8. Reference path generation

Finally the reference to feed the controller is obtained from the reference path B-spline, assuming an external total speed command $V_R$, using the following procedure:

- compute the vehicle closest point on the path $(x_R, y_R)$, and the respective arc length parameter $l_R$ such that $(x_R, y_R) = (x(l_R), y(l_R))$;
- obtain the reference angular velocity from $r_R = \kappa(l_R)\, V_R$, where $\kappa(l_R)$ is the local curvature at the closest point defined by

$$\kappa(l_R) = \frac{x''(l_R)\, y'(l_R) - y''(l_R)\, x'(l_R)}{(x'(l_R)^2 + y'(l_R)^2)^{3/2}};$$

- compute the angle of the tangent frame at the closest point $\psi_T(l_R) = \mathrm{atan2}(x'(l_R), y'(l_R))$, where $\mathrm{atan2}(.,.)$ denotes the four quadrant arctangent function.

## IMPLEMENTATION

The design and performance evaluation of the overall closed loop system were carried out using the model described in Section II.

During the controller design phase the ASC's operation envelope was parameterized by $\boldsymbol{\xi} = [V_R, r_R]^T$ and partitioned into 25 regions resulting from the parameter intervals presented in Table I. For each operating region, the elements of the discrete time state space matrices were obtained from the linearization of the error dynamics over a dense

Table I. Parameter intervals

| Parameters | Intervals |
|---|---|
| $V_R\ [m.s^{-1}]$ | [0.4;0.5] [0.45;1] [0.8;1.5] [1.3;2] [1.8;2] |
| $r_R\ [rad.s^{-1}]$ | [-0.01;0.01] [0.008;0.02] [0.018;0.022] [-0.02;-0.008] [-0.022;-0.018] |

grid of operating points and then approximated by affine functions of $\boldsymbol{\xi}$ using a Least Squares Fitting.

To implement the controller within the scope of gain scheduling control theory, a state feedback gain matrix $\mathrm{K}_i = [\mathrm{K}_{di},\ \mathrm{K}_{si}],\ i = 1, \ldots, 25$ was computed for each of the operating regions using the technique presented in Section V. During the controller design phase the regions were defined so as to overlap thus avoiding fast switching between controllers. In the synthesis model (11) the disturbance input matrix $B_w$ was set to $\bar{B}_s$ and the state and control weight matrices $C_z$ and $E$, respectively, were set to yield the following performance vector $\mathbf{z}(k) = [\mathbf{z}_1(k)^T\ \mathbf{z}_2(k)^T]^T$, where

$$\mathbf{z}_1 = [0.01u_e, 0.1v_e, r_e, 0.1d_t, \psi_e, 0.03x_{i1}, 0.15x_{i2}]^T$$
$$\mathbf{z}_2 = [0.15n_c, 0.1n_d]^T\ ,$$

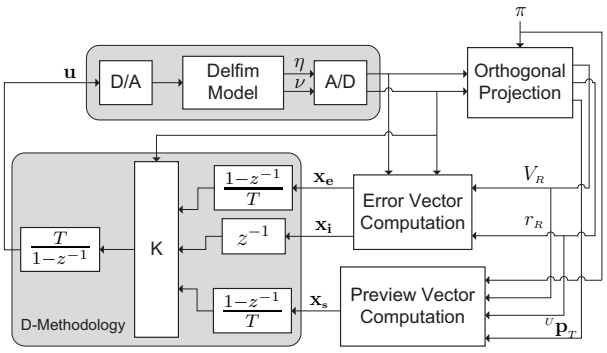


Fig. 9. Implementation setup using gain scheduling and the D-methodology

The final implementation scheme, presented in Fig. 9, was achieved using the D-methodology described in (Kaminer *et al.*, 1995). Besides preserving the stability characteristics of the closed loop system, this methodology has the important property of eliminating the need to feedforward trimming values for the actuation signals and state variables that are not required to track reference inputs.

The width of the preview interval suitable for a given vehicle is a compromise between the time-constants associated to the vehicle's dynamics and the computational power available onboard. Fig. 10 presents the entries of the preview feedforward control matrix $K_s$ as a function of the preview time, obtained for zone 2. In this case, a preview interval of $25\,\mathrm{s}$, sampled at $T = 0.5\,\mathrm{s}$, is considered. It is clear that the weight of the preview signal decreases as the corresponding instant of time gets further ahead in the future, with negligible contributions above $25\,\mathrm{s}$ of preview time.

The computation of the reference path was obtained with $\alpha = 5$, and $0.5$ m step for both spline generation and coefficient estimation points and an equally spaced knot vector with $1$ m step. In the simulation the nominal laser range finder measurements were assumed corrupted by additive white noise with variance $0.5\,\mathrm{m}^2$.

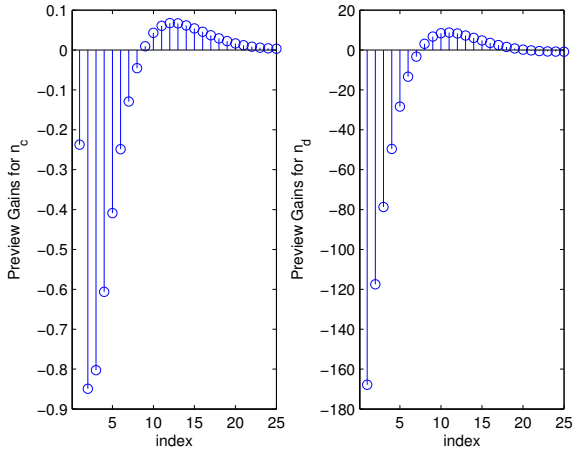


Fig. 10. Evolution of the preview gains as a function of preview time

## SIMULATION RESULTS

In this section, we illustrate the performance that can be achieved with the proposed coast following controller. In the simulation the catamaran DELFIMx should follow the coastline at a constant reference speed of $V_R = 1.5$ m/s. As shown in Figs. 11, 12, and 13, the inclusion of preview feedforward control action yields better path-following performance, since it results in a smoother path trajectory with reduced convergency time. Notice that there is a starting path, which corresponds to a straight line, for laser points accumulation in the data buffer. The effect of the use of preview becomes clear from Figs. 14 and 15, as the changes in the trajectory described by the vehicle impact on the coastline following capabilities.

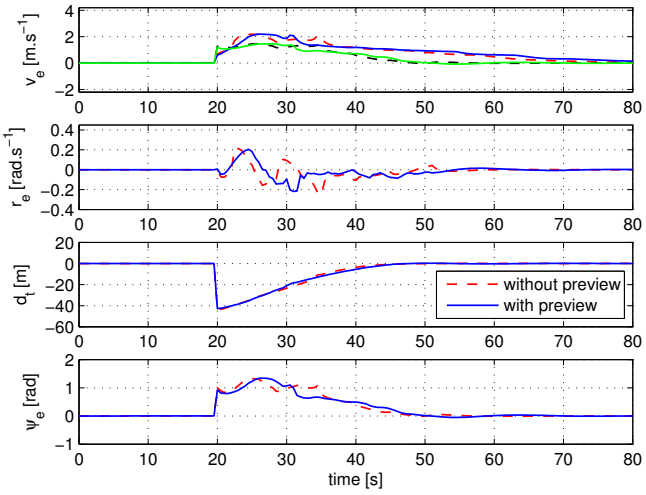


Fig. 11. Time evolution of the error vector

## CONCLUSIONS

The paper presented the design and performance evaluation of a coast following controller for an Autonomous Surface Craft (ASC). Resorting to an $H_2$ controller design methodology for affine parameter-dependent systems, the technique presented exploited an error vector that naturally describes the dynamic characteristics of the ASC for a suitable flight envelope. For a given set of operating regions, a nonlinear preview controller was synthesized and implemented under the scope of gain-

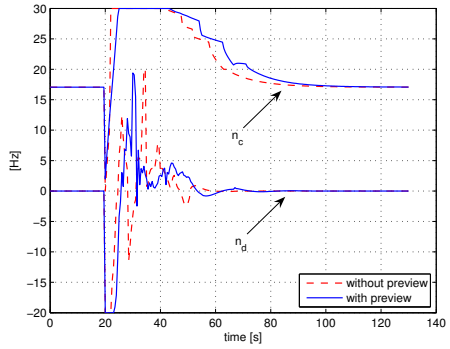


Fig. 12. Time evolution of the actuation

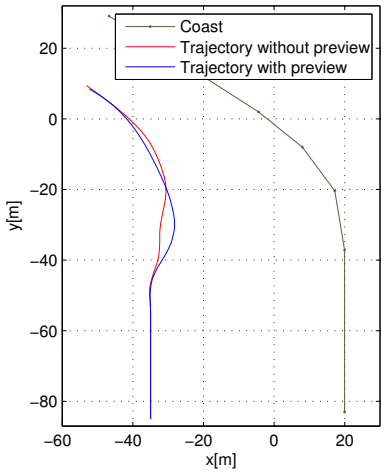


Fig. 13. Trajectories described by the vehicle

scheduling control theory.

The effectiveness of the new control laws was assessed in simulation, using a nonlinear model of the DELFIMx catamaran with a laser range finder installed on board. A new technique was proposed to generate a smooth reference path from laser data. The quality of the results obtained in simulation clearly indicate that the methodology proposed yields a high-performance coast following preview controller that has great potential to be used in practical applications.

## REFERENCES


Cunha, R., D. Antunes, P. Gomes and C. Silvestre (2006). A path-following preview controller for autonomous air vehicles. In: *AIAA GNC Conference*. Keystone, CO.

de Boor, Carl (2001). *A practical guide to splines*. Applied Mathematical Science, Springer. New York, USA.

Farin, G. (1997). *Curves and Surfaces for Computer-aided Geometric Design: A Practical Guide*. 4th Ed. Academic Press. San Diego, USA.

Flickner, M., J. Hafner, EJ Rodriguez and JLC Sanz (1994). Fast least-squares curve fitting using quasi-orthogonal splines. *Image Processing, 1994. Proceedings. ICIP-94., IEEE International Conference*.

Ghaoui, L. El and Niculescu, S. I., Eds.) (1999). *Advances in Linear Matrix Inequality Methods in Control*. SIAM. Philadelphia.

Kaminer, I., A. Pascoal, P. Khargonekar and E. Coleman (1995). A velocity algorithm for the implementation of gain-sheduled controllers. *Automatica*.


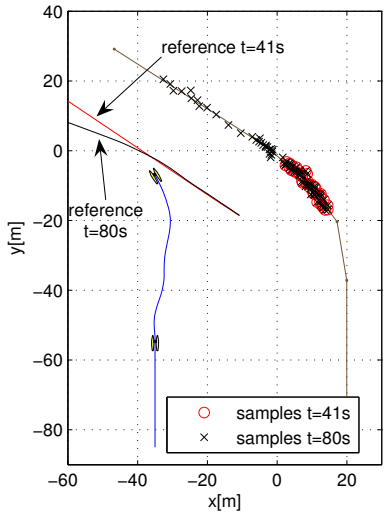


Fig. 14. Reference paths without preview

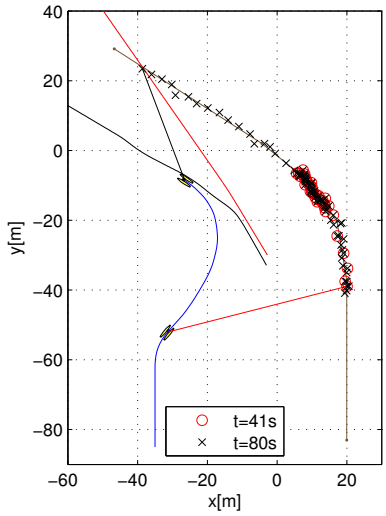


Fig. 15. Reference paths with preview


Lee, I.K., M.S. Kim and G. Elber (1996). Planar curve offset based on circle approximation. *Computer-Aided Design* **28**(8), 617–630.

Paulino, N., C. Silvestre and R. Cunha (2006). Affine parameter-dependent preview control for rotorcraft terrain following flight. *AIAA Journal of Guidance, Control, and Dynamics*.

Prado, M. (2002). Modeling and control of an autonomous oceanographic vehicle. Master's thesis. Instituto Superior Técnico, Lisbon.

Silvestre, Carlos, Paulo Oliveira, António Pascoal, Luís Gabriel Silva, João Alfredo Santos and Maria da Graça Neves (2004). Inspection and diagnosis of the sines west breakwater. In: *ICCE2004 29th, International Conference on Coastal Engineering*. Lisboa.

Takaba, K. (2000). Robust servomechanism with preview action for polytopic uncertain systems. *International Journal of Robust Nonlinear Control* **10**, 101–111.

Tomizuka, M. (1976). Optimum linear preview control with applications to vehicle suspension-revisited. *ASME Journal of Dynamic Systems, Measurement and Control, Vol.98, pp. 309-315*.

Zhou, K., J. C. Doyle and K. Glover (1995). *Robust and Optimal Control*. Prentice Hall. New Jersey.